Photochemically induced dynamic nuclear polarization in Photosystem I of plants observed by 13C magic-angle spinning NMR

Alia, A.; Roy, E.; Gast, P.; Gorkom, H.J. van; Groot, H.J.M. de; Jeschke, G.; Matysik, J.

J|A|C|S
ARTICLES
Published on Web 09/18/2004

Photochemically Induced Dynamic Nuclear Polarization in Photosystem I of Plants Observed by ^{13}C Magic-Angle Spinning NMR

Alia,[†] Esha Roy,[†] Peter Gast,[‡] Hans J. van Gorkom,[‡] Huub J. M. de Groot,[†] Gunnar Jeschke,[§] and Jörg Matysik*,[†]

Contribution from the Leiden Institute of Chemistry, Gorlaeus Laboratoria, P.O. Box 9502, 2300 RA Leiden, The Netherlands, Department of Biophysics, Huygens Laboratory, P.O. Box 9504, 2300 RA Leiden, The Netherlands, and Max-Planck-Institut für Polymerforschung, Postfach 3148, 55021 Mainz, Germany

Received April 5, 2004; E-mail: j.matysik@chem.leidenuniv.nl

Abstract: Photochemically induced dynamic nuclear polarization (photo-CIDNP) has been observed in photosystem I of spinach by ^{13}C magic angle spinning solid-state NMR under continuous illumination with white light. An almost complete set of chemical shifts of the aromatic ring carbons of a single Chl *a* molecule has been obtained which is assigned to the P2-cofactor of the primary electron donor P700. Since all light-induced ^{13}C NMR signals appear to be emissive, a predominance of the three-spin mixing mechanism over the differential decay mechanism is proposed. The origin of the strong contribution of the three-spin mixing mechanism and the differences with photosystem II are discussed.

Introduction

Photosynthesis in plants is driven by light-induced electron transfer in the two reaction centers (RCs), photosystem I (PS1)[1] and photosystem II (PS2).[2] Whereas the oxidized primary electron donor of PS2, $P680^{\bullet+}$, is a very powerful oxidizing agent, even allowing to oxidize water, the electronically excited primary electron donor of PS1, P700*, is a strong reducing agent. The coupling of both light-driven electron pumps allows plants to reduce CO_2 during the Calvin cycle by using reduction equivalents obtained from H_2O oxidation. The origin of the different redox properties of both RCs is not yet clear.

Recently, an X-ray structure of PS1 from the thermophilic cyanobacterium *Synechococcus elongatus* at a resolution of 2.5 Å has been published (Figure 1).[3,4] The 3-dimensional structure shows that P700 is a heterodimer formed by one chlorophyll *a* (Chl *a*) molecule and one chlorophyll *a*′ (Chl *a*′) molecule, which is the C13[2]-epimer of Chl *a*. Due to their 5-coordination, both Chl macrocycles are domed. The interplanar distance between both macrocycles is 3.6 ± 0.3 Å. Corresponding pyrrole rings I and II are partially overlapping. Chl *a*′ forms hydrogen bonds to its environment, no hydrogen bonds are found on the Chl *a* side. In comparison to the special pair of purple bacterial RCs (for review, see ref 5), the *spatial* structure of P700 appears to be quite asymmetric. The *electronic* structure of P700 remains under discussion (for review, see ref 6). The available spectroscopic data are mainly from vibrational and electron magnetic resonance spectroscopic methods. The spectroscopic observation of a broad mid-IR transition[7,8] in the oxidized and paramagnetic $P700^{\bullet+}$ is generally interpreted as proof for charge repartition over two Chl cofactors, called P1 and P2. As concluded from

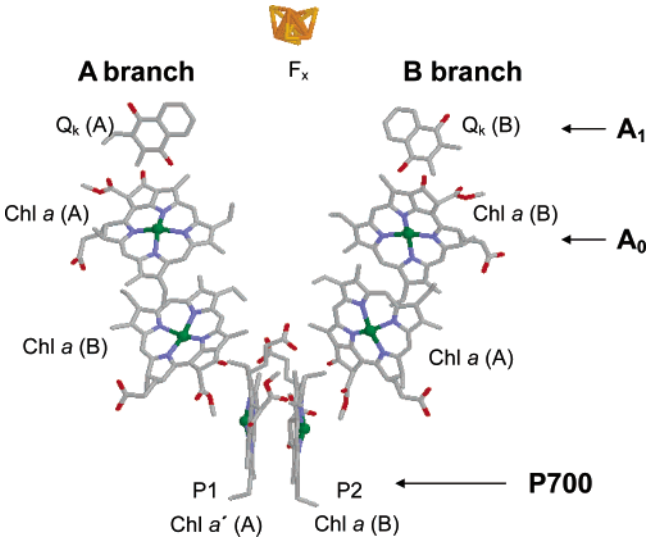

Figure 1. Arrangement of cofactors in the RC of PS1.[4] The aliphatic side chains of the cofactors have been omitted for clarity.

[†] Gorlaeus Laboratoria.
[‡] Huygens Laboratory.
[§] Max-Planck-Institut für Polymerforschung.

(1) Brettel, K.; Leibl, W. *Biochim. Biophys. Acta* **1997**, *1507*, 100−114.
(2) Diner, B. A.; Rappaport, F. *Annu. Rev. Plant Biol.* **2002**, *53*, 551−580.
(3) Fromme, P.; Jordan, P.; Krauss, N. *Biochim. Biophys. Acta* **2001**, *1507*, 5−31.
(4) Jordan, P.; Fromme, P.; Witt, H. T.; Klukas, O.; Saenger, W.; Krauss, N. *Nature* **2001**, *411*, 909−917.
(5) Hoff, A. J.; Deisenhofer, J. *Physics Reports* **1997**, *287*, 2−247.
(6) Webber, A. N.; Lubitz, W. *Biochim. Biophys. Acta* **2001**, *1507*, 61−79.
(7) Breton, J. *Biochim. Biophys. Acta* **2001**, *1507*, 180−193.
(8) Hastings, G.; Ramesh, V. M.; Wang, R.; Sivakumar, V.; Webber, A. *Biochemistry* **2001**, *40*, 12943−12949.

the C═O stretching vibrations, P1 is hydrogen-bonded on both keto-functions and can be assigned to the Chl *a*′. It carries all of the triplet character of ^{3}P700, while the carbonyl groups of P2 are free from hydrogen bonding interaction.[9] Mutant studies provide evidence for electronic coupling between the two halves of the dimer.[10] Data from different electron magnetic resonance spectroscopies, i.e., electron paramagneticresonance (EPR),[11−13] electron−nuclear double resonance (ENDOR),[13−20] and electron-spin−echo-envelope-modulation (ESEEM),[21−25] have been interpreted quite differently. Originally, a symmetric dimer[11,16] and a Chl monomer[15] were proposed. More recently, an asymmetric dimer has been proposed,[18,19] in which the second Chl (P1) carries about ≤15% of the spin density.[20] A very recent molecular orbital study based on the 2.5 Å structure indeed described P700 as dimer with an asymmetric electron spin density distribution in favor of the monomeric Chl *a* (P2) half by a spin density ratio of almost 5:1.[26] Information on the electron spin density distribution and the electronic ground state at atomic resolution are however missing.

Magic-angle spinning (MAS) solid-state NMR is a powerful method for studying structure and dynamics of membrane proteins.[27] In principle, NMR chemical shift information can allow for the exploration of spatial, protonic, and electronic structures at atomic resolution in the electronic ground state. Such analysis can provide detailed insight into functional mechanisms of proteins. In the case of several photosynthetic RCs of bacteria and plants, it has been shown that photochemically induced dynamic nuclear polarization (photo-CIDNP) can overcome the intrinsic insensitivity and nonselectivity of NMR spectroscopy by photochemical induction of non-Boltzmann population of nuclear spin states. Photo-CIDNP has been observed for the first time in quinone blocked bacterial RCs from *Rhodobacter* (*Rb*.) *sphaeroides* R26[28,29,30,31] and wildtype (WT).[32] The strong enhancement by the combination of selective ^{13}C-isotope labeling at several cofactor positions and photo-CIDNP allowed us to obtain two-dimensional photo-CIDNP MAS NMR spectra, which demonstrated that the electron density of the two BChl molecules of the special pair is already different in the electronic ground state of the bacterial RC.[33] Furthermore, NMR signals were detected in entire membrane-bound bacterial photosynthetic units (>1.5 MDa).[34] In the D1D2 complex of the RC of photosystem II of plants, the observation of the pronounced electron spin density on rings III and V by photo-CIDNP MAS NMR was taken as an indication for a local electric field, leading to a hypothesis about the origin of the remarkable strength of the redox potential of the primary electron donor P680.[35]

In addition to the information on the electronic ground state provided by the NMR chemical shifts, photo-CIDNP solid-state NMR intensities are linked to the local electron spin densities occurring in the radical-pair state. As electron transfer is a spin-conserving process, the electron pair is initially in a singlet state, which corresponds to nonequilibrium enhanced spin polarization for the pair. Due to the coupling between the two electron spins, this pair polarization evolves to enhanced polarization of the two constituent radical ions, which is then transferred to polarization of the nuclear spins by an anisotropic hyperfine coupling in a process denoted three-spin mixing mechanism (TSM).[36,37] Alternatively, in the differential decay mechanism (DD), the polarization of the constituent radical ions can arise from evolution to a superposition of the singlet and triplet state of the pair due to different *g* values and hyperfine couplings of the two electron spins and subsequent preferential decay of pairs in a triplet state.[38] Again, the electron polarization is then transferred to nuclear polarization by an anisotropic hyperfine coupling. Photo-CIDNP intensities, which are proportional to the nuclear polarization, thus depend strongly on the anisotropy of the hyperfine coupling. The exact link between the local electron-spin densities and the photo-CIDNP intensities, however, remains the object of further studies since the mechanism producing photo-CIDNP in solids is currently under discussion.[39]

In PS1, light-induced electron spin polarization has been observed for the first time[40] in 1975 (for recent review, see ref 41). The rise of nuclear coherence has been observed as nuclear quantum beat oscillations.[42,43] Here, we present the first photo-CIDNP data of PS1, observed by ^{13}C MAS NMR.

Materials and Methods

Photosystem I Particle Preparation. The PS1 complex containing ~110 Chl/P700 was prepared from spinach according to Mullet et al.[44]

(9) Breton, J.; Nabedryk, E.; Leibl, W. *Biochemistry* **1999**, *38*, 11585−11592.
(10) Witt, H.; Schlodder, E.; Teutloff, C.; Niklas, J.; Bordignon, E.; Carbonera, D.; Kohler, S.; Labahn, A.; Lubitz, W. *Biochemistry* **2002**, *41*, 8557−8569.
(11) Norris, J. R.; Uphaus, R. A.; Crespi, H. L.; Katz, J. J. *Proc. Natl. Acad. Sci. U.S.A.* **1971**, *68*, 625−628.
(12) Norris, J. R.; Druyan, M. E.; Katz, J. J. *Am. Chem. Soc.* **1973**, *95*, 1680−1682.
(13) Norris, J. R.; Scheer, H.; Druyan, M. E.; Katz, J. *Proc. Natl. Acad. Sci. U.S.A.* **1974**, *71*, 4897−4900.
(14) Hoff, A. J. *Phys. Rep.* **1979**, *54*, 75−200.
(15) O'Malley, P. J.; Babcock G. T. *Proc. Natl. Acad. Sci. U.S.A.* **1984**, *81*, 1098−1101.
(16) Norris, J. R.; Scheer, H.; Katz, J. *Ann. New York Acad. Sci.* **1975**, *244*, 260−280.
(17) Lendzian, F.; Lubitz, W.; Scheer, H.; Hoff, A. J.; Plato, M.; Trankle, E.; Möbius, K. *Chem. Phys. Lett.* **1988**, *148*, 377−385.
(18) Rigby, S. E. J.; Nugent, J. H. A.; O'Malley, P. J. *Biochemistry* **1994**, *33*, 10043−10050.
(19) Krabben, L.; Schlodder, E.; Jordan, R.; Carbonera, D.; Giacometti, G.; Lee, H.; Weber, A. N.; Lubitz W. *Biochemistry* **2000**, *39*, 13012−13025.
(20) Käss, H.; Fromme, P.; Witt, H. T.; Lubitz W. *J. Phys. Chem. B* **2001**, *105*, 1225−1239.
(21) Käss, H.; Bittersmann-Weidlich, E.; Andreassson, L.-E.; Bönigk, B.; Lubitz, W. *Chem. Phys.* **1995**, *194*, 419−432.
(22) Käss, H.; Lubitz W. *Chem. Phys. Lett.* **1996**, *251*, 193−203.
(23) Käss, H.; Fromme, P.; Lubitz, W. *Chem. Phys. Lett.* **1996**, *257*, 197−206.
(24) Mac, M.; Tang, X.-S.; Diner, B. A.; McCracken, J.; Babcock G. T. *Biochemistry* **1996**, *35*, 13288−13293.
(25) Käss, H.; Lubitz, W.; Hartwig, G.; Scheer, H.; Noy, D.; Scherz A. *Spectrochim. Acta A* **1998**, *54*, 1141−1156.
(26) Plato, M.; Krauss, N.; Fromme, P.; Lubitz W. *Chem. Phys.* **2003**, *294*, 483−499.
(27) de Groot, H. J. M. *Curr. Opin. Struct. Biol.* **2000**, *10*, 593−600.
(28) Zysmilich, M. G.; McDermott, A. E. *J. Am. Chem. Soc.* **1994**, *116*, 8362−8363.
(29) Zysmilich, M. G.; McDermott, A. E. *J. Am. Chem. Soc.* **1996**, *118*, 5867−5873.
(30) Zysmilich, M. G.; McDermott, A. E. *Proc. Natl. Acad. Sci. U.S.A.* **1996**, *93*, 6857−6860.
(31) Matysik J.; Alia; Hollander, J. G.; Egorova-Zachernyuk, T.; Gast, P.; de Groot, H. J. M. *Indian J. Biochem. Biophys.* **2000**, *3*, 418−423.
(32) Matysik, J.; Alia; Gast, P.; Lugtenburg, J.; Hoff, A. J.; de Groot, H. J. M.; In *Perspectives on Solid State NMR in Biology*; Kiihne, S., de Groot, H. J. M., Eds.; Kluwer: Dordrecht, 2001; p 215−225.
(33) Schulten, E. A. M.; Matysik, J.; Alia; Kiihne, S.; Raap, J.; Lugtenburg, J.; Gast, P.; Hoff, A. J.; de Groot, H. J. M. *Biochemistry* **2002**, *41*, 8708−8717.
(34) Prakash, S.; Alia; Gast, P.; Jeschke, G.; de Groot, H. J. M.; Matysik J. *J. Mol. Struc.* **2003**, *661−662*, 625−633.
(35) Matysik, J.; Alia; Gast, P.; van Gorkom, H. J.; Hoff A. J.; de Groot, H. J. M. *Proc. Natl. Acad. Sci. U.S.A.* **2000**, *97*, 9865−9870.
(36) Jeschke, G. *J. Chem. Phys.* **1997**, *106*, 10072−10086.
(37) Jeschke, G. *J. Am. Chem. Soc.* **1998**, *120*, 4425−4429.
(38) Polenova, T.; McDermott, A. E. *J. Phys. Chem. B* **1999**, *103*, 539−548.
(39) Jeschke, G.; Matysik, J. *Chem. Phys.* **2003**, *294*, 239−255.
(40) Blankenship, R.; McGuire, A.; Sauer, K. *Proc. Natl. Acad. Sci. U.S.A.* **1975**, *72*, 4943−4947.
(41) van der Est, A. *Biochim. Biophys. Acta* **2001**, *1507*, 212−225.
(42) Weber, S.; Ohmes, E.; Thurnauer, M. C.; Norris, J. R.; Kothe G. *Proc. Natl. Acad. Sci. U.S.A.* **1995**, *92*, 7789−7793.
(43) Kothe, G.; Bechtold, M.; Link, G.; Ohmes, E.; Weidner J.-U. *Chem. Phys. Lett.* **1998**, *283*, 51−60.

First the chloroplasts were isolated by grinding excised leaves in 0.4 M Sorbitol and 50 mM Tricine buffer (pH 7.8) as previously described.[45] Isolated chloroplasts were washed once with 10 mM Tricine buffer (pH 7.8) containing 50 mM Sorbitol and 5 mM EDTA and then re-suspended in 10 mM Tricine buffer (pH 7.8) to obtain a final concentration of 0.8 mg Chl/mL. The membranes (0.8 mg/mL) were solubilized with Triton X-100 (final concentration of 0.8% w/v) for 30 min at room temperature in the dark with continuous slow stirring. The solubilized membranes were centrifuged at 39 000 g for 20 min at 4 °C and the supernatant fraction was loaded onto a linear sucrose gradient (0.1−1.0 M sucrose, 10 mM Tricine, 0.02% Triton X-100, pH 7.8) prepared on a 2 M sucrose cushion followed by ultracentrifugation at 150 000 g for 18 h at 4 °C. PS1−110 particles showed up as a dark green nonfluorescent band just above the 2 M sucrose cushion. After collecting this band, the PS1−110 particles were dialyzed overnight against 10 mM Tricine and were concentrated by centrifugation at 150 000 g for 16 h. PS1−110 particles were finally suspended in 5 mM Tricine buffer (pH 7.8) containing 50 mM Sorbitol. The chlorophyll content of PS1−110 was determined by the method of Arnon et al.[46] PS1−110 particles equivalent to ∼2 mg Chl/mL were used for NMR measurements.

CPI particles (PS1 particles containing ∼40 Chl/P700 and lacking the ferredoxin acceptors F_X, F_B, F_A) were prepared using a modification of the method of Rutherford and Mullet.[47] In brief, the PS1−110 particles (1 mg Chl/mL) were incubated with 2% lithium dodecyl sulfate (LDS) for 1 h at 4 °C. Subsequently, the particles were loaded on a linear sucrose gradient (0.1−1 M sucrose, 10 mM Tricine, 0.1% sodium cholate, pH 8) and centrifuged at 150 000 g for 16 h. The CPI particles appeared as a dark green band about 2 cm from the bottom of the centrifuge tube. After removal of this band, the CPI particles were dialyzed overnight against 10 mM Tricine and were concentrated by centrifugation at 150 000 g for 16 h.

The PS1−110 particles and CPI particles were highly pure as has been analyzed by SDS gel electrophoresis. PSI-110 was resolved into 12 clearly distinguishable bands (68, 66, 24.5, 24, 22.0, 22.5, 21, 17, 16.5, 11.5, 11.0, and 10.5 kDa) corresponding to at least 8 Psa and 4 Lhca polypeptides. This pattern was similar as has been published earlier by Mullet et al.[44] CPI particles were resolved into two bands (66 and 68 kDa) corresponding to PsaA and PsaB polypeptides.[48]

MAS NMR Measurements. The NMR experiments have been performed using a DMX-400 NMR spectrometer (Bruker GmbH, Karlsruhe, Germany) equipped with a triple-resonance magic angle spinning (MAS) light probe working at 396.5 MHz for protons and 99.7 MHz for ^{13}C. The samples were loaded into optically transparent 4 and 7-mm sapphire rotors. Reduction of ferredoxin acceptors F_B and F_A in PS1−110 particles was performed by addition of an aqueous solution of 10 mM sodium dithionite solution and 40 mM glycine buffer (pH 9.5) in an oxygen free atmosphere. Immediately following the reduction, slow freezing of the sample was performed directly in the NMR probe inside the magnet with liquid-nitrogen-cooled gas under continuous illumination with white light using an illumination setup specially designed for the Bruker MAS probe.[31,32] During this slow freezing, the sample was spinning slowly (∼600 Hz) to ensure a homogeneous sample distribution against the rotor wall. Photo-CIDNP ^{13}C MAS NMR spectra were obtained at a temperature of 223 K under continuous illumination. To distinguish the centerbands from the spinning sidebands, photo-CIDNP MAS NMR spectra were recorded at different spinning frequencies, 3.6, 4.0, 5.0, 6.4, 8.0, and 9.0 kHz. The light and dark spectra have been collected by a straightforward

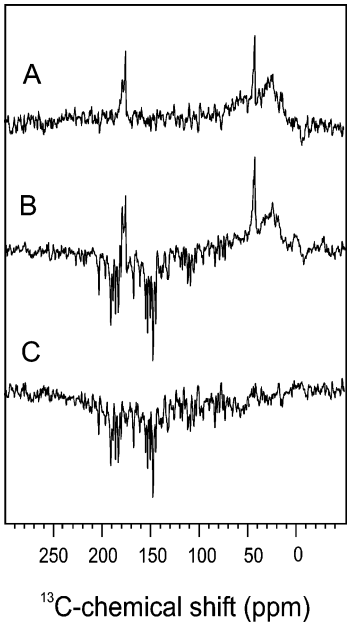

Figure 2. ^{13}C MAS NMR spectra of PS1−110 particles at 223K and a MAS frequency of 3.6 kHz. Spectra are obtained A: in the dark, B: under continuous illumination with white light, C: by subtraction B − A.

Bloch decay followed by a Hahn echo and two pulse phase modulation (TPPM) proton decoupling.[49] A recycle delay of 12 s was used, and a total number of 14 000 scans per spectrum was collected over a period of 48 h.

DFT Computations. All density functional computations were performed with ADF 2002.01.[50] Three different Chl structures were tested: A structure obtained from X-ray data,[51] which was used without further optimization, a structure based on standard bond angles and bond lengths,[52] and an optimized starting structure of a bacteriochlorophyll *a* (BChl *a*). The latter was edited in Titan 1.0 (Wave function Inc., Irvine, CA) to give the structure of Chl *a* in PS1 shown in Figure 5, with residue R substituted by a methyl group to save computation time. This structure was then optimized within ADF (basis set DZP for all atoms, frozen core up to 1 s for C,N,O and up to 2 p for Mg). A structure of an analogous pheophytin *a* (Pheo *a*) was then obtained by deleting the Mg^{2+} ion and adding two hydrogens in Titan 1.0. This procedure allows for simple comparison of the principal axis frames of *g* tensors, which were computed for the optimized structure of the Chl *a* anion radical and the analogous pheophytin anion radical within the spin-restricted zeroth order relativistic approximation (ZORA) formalism with all-electron basis sets DZP for all atoms.[53,54] A nonrelativistic spin-unrestricted computation with all-electron TZ2P basis set on all atoms gave the hyperfine tensors of Chl *a* cation and anion radicals.

Results

Figure 2 shows ^{13}C MAS NMR spectra of natural abundance PS1−110 particles in the dark (A) and under continuous illumination with white light (B). Spectrum 2A shows the

(44) Mullet, J. E.; Burke, J. J.; Arntzen, C. J. *Plant Physiol.* **1980**, *65*, 814−822.
(45) Arntzen, C. J.; Ditto, C. L. *Biochim. Biophys. Acta* **1976**, *449*, 259−274.
(46) Arnon, D. I. *Plant Physiol.* **1949**, *24*, 1−15.
(47) Rutherford, A. W.; Mullet, J. E. *Biochim. Biophys. Acta* **1981**, *635*, 225−235.
(48) Gast, P.; Swarthoff, T.; Ebskamp, F. C. R.; Hoff, A. J. *Biochim. Biophys. Acta* **1983**, *722*, 163−175.
(49) Bennet, A. E.; Rienstra, C. M.; Auger, M.; Lakshmi, K. V.; Griffin, R. G. *J. Chem. Phys.* **1995**, *103*, 6951−6958.
(50) Velde, G. T.; Bickelhaupt, F. M.; Baerends, E. J.; Fonseca Guerra, C.; van Gisbergen, S. J. A.; Snijders, J. G.; Ziegler, T. *J. Comput. Chem.* **2001**, *22*, 931−967.
(51) Chow, H. C.; Serlin, R.; Strouss C. E. *J. Am. Chem. Soc.* **1975**, 97, 7230−7237.
(52) Käss, H.; Rautter, J.; Bönigk, B, Höfer, P.; Lubitz, W. *J. Phys. Chem.* **1995**, 99, 436−448.
(53) van Lenthe, E.; Snijders, J. G.; Baerends, E. J. *J. Chem. Phys.* **1996**, *105*, 6505−6516.
(54) van Lenthe, E.; van der Avoird, A.; Wormer, P. E. S. *J. Chem. Phys.* **1998**, *108*, 4783−4796.

Table 1. ^{13}C Chemical Shifts of the Photo-CIDNP Signals Obtained at 9.4 T in Comparison to Published Chemical Shift Data for Chlorophyll *a*

chemical shifts				
Chl *a*		assignment	PS2	PS1
σ_{liq}[a]	σ_{ss}[b]	atom	σ[c]	σ[d]
189.3	190.6	13^1		~190.6 E
172.7	175.3	17^3		
171.0	171.2	13^3		
167.4	170.0	19	166.9 A	167.1 E
161.4	162.0	14	162.3 A	160.4 E
154.0	155.9	1	156.0 A	154.8 E
155.8	154.4	6		
151.4	154.0	16	151.7 A	152.6 E
148.0	150.7	4		149.9 E
147.7	147.2	11	147.7 A	147.2 E
146.1	147.2	9		
144.1	146.2	8		144.2 E
139.0	137.0	3	137.5 A	138.6 E
135.5	136.1	2		~136 E
134.2	134.0	12		
134.0	133.4	7	133.9 A	~132 E
131.5	126.2	13		
131.5	126.2	3^1		
118.9	113.4	3^2		
107.1	108.2	10	104.6 E	105.4 E
106.2	102.8	15		
100.0	98.1	5		
92.8	93.3	20		

[a] Abraham and Rowan (1991). The liquid NMR data have been obtained in tetrahydrofuran. [b] Boender (1991). The solid-state NMR data have been obtained from aggregates. [c] Matysik et al. (2001). [d] This work. Abbreviations: σ = chemical shift, A = absorptive signal, E = emissive signal

characteristic aliphatic features of a ^{13}C-MAS NMR spectrum of a protein, i.e., a broad response between 0 and 50 ppm. The sharp signals at 175.7 and 41.9 ppm arise from glycine, which has been added as a cryoprotectant. The relatively broad signal at 179 ppm contains intensity of the protein carbonyl groups. In spectrum 2B, several strong emissive (negative) signals appear upon illumination. It is indeed remarkable to observe NMR signals of such intensity from the active site of a large membrane protein complex, containing 110 Chls. Photo-CIDNP enhancement has only been observed in PS1−110 and PS1−CPI particles which were prereduced. The difference spectrum 2C shows that all of the light-induced signals appear exclusively in the aromatic region.

In the spectra of the PS1−110 preparation, a total of 12 centerbands that are independent of the rotational frequency (spectra 3A−C) have been identified. Using the chemical shifts of monomeric and aggregated Chl *a* from the literature, these centerbands can be tentatively assigned to 17 carbon atoms of a single Chl *a* cofactor (Table 1). Future experiments on carbon labeled Chl *a* cofactors may provide definite assignments. There is no evidence for signal doubling in the spectrum. An alternative assignment to a Phe *a* is not possible since the RC of PS1 does not contain Phe *a* cofactors. In the carbonyl region, the carbon C-13^1 is detected as a relatively broad signal at 190.6 ppm. The strongest signals are observed in the aromatic region between 120 and 170 ppm. The signal at 154.8 ppm shows a shoulder and can be assigned to both C-1 and C-6. The strong signal at 147.2 ppm is assigned to C-9 and C-11, which is in line with previous MAS NMR experiments on precipitated Chl *a* molecules, where these two signals are also not separated.[55] Also the three carbons C-2, C-4, and C-8 can be detected which have not yet been observed in PS2. The broad signal at ≈133 ppm can be assigned to the carbons C-7, C-12, and C-13. The response at ≈105.4 ppm can be assigned to both the C-10 and C-15 methine carbons. As in PS2, the methine carbons C-5 and C-20 are not detected. No light induced signal is observed in the region of the aliphatic carbons. In bacterial RCs, emissive signals at about 118.5 and 134 ppm have been assigned to an axial histidine ligand of the special pair.[56,57] This contrasts with the data for the PS1, since all twelve centerbands can be conveniently assigned to a single Chl-*a* cofactor.

At moderately fast MAS, spinning sidebands are observed at integral multiples of the rotational frequency, relative to the centerband. These bands contain information about the chemical shift anisotropy (CSA), i.e., the asymmetry of the diamagnetic susceptibility associated with the ground-state electron density distribution. Using the method of Herzfeld and Berger,[58] the CSA for several of the strongest signals with centerbands between 130 and 180 ppm were found to be similar to the anisotropies measured for solid Chl *a* and to be characteristic for aromatic systems.

The intensity of the photo-CIDNP signals of PS1−110 is very strong relative to the dark background. The strongest photo-CIDNP signals have about three times the intensity of the maximum of the aliphatic signals at 30 ppm. This is similar to the ratio observed from the best preparations of RCs of bacteria and of PS2 in D1D2. The molecular mass of the PS1−110 preparation (≈300 kDa) is approximately a factor three larger. This means that PS1−110 shows the most intense photo-CIDNP signals ever observed in an unlabeled RC. This effect can be partially, but not exclusively attributed to the relatively narrow line width of 60−65 Hz, which is less than the line widths of 80 to 100 Hz that are observed for PS2.

The spectrum obtained from the PS1−CPI preparation shows the same center bands with a similar intensity pattern as found in PS1−110 at the same spinning frequency (Figure 4). The signal at 154.8 ppm, which is assigned to both C-1 and C-6, however, is clearly reduced. Furthermore, the line width of all signals is significantly increased. These effects indicate increased heterogenity of the sample compared to the PS1−110 preparation probably due to the removal of subunits. The removal of surrounding antenna apparently destabilizes the RC.

Discussion

The Radical Pair. In the illumination experiments, a P_{700}^+ A_0^- radical pair is formed.[59] Photo-CIDNP enhancement has only been observed in reduced PS1−110 and PS1−CPI particles. In CPI-particles, the ferrodoxins are removed, which suggests that the quinone has to be reduced to obtain photo-CIDNP. The radical pair P_{700}^+ A_1^-, which is produced upon illumination in samples without prereduction by sodium dithionite, does not produce photo-CIDNP, presumably because the electron−electron coupling is too weak. On the other hand, under strong permanent illumination, also the Chl *a* of the second pair of Chl *a* molecules next to P700, can become photoreduced.[59] Since this radical pair is tightly coupled and

(55) Boender, G. J. Ph.D. Thesis, University of Leiden, The Netherlands, 1996.
(56) Alia; Matysik, J.; Soede-Huijbregts, C.; Baldus, M.; Raap, J.; Lugtenburg, J.; Gast, P.; van Gorkom, H. J.; Hoff, A. J.; de Groot, H. J. M. *J. Am. Chem. Soc.* **2001**, *123*, 4803−4809.
(57) Matysik, J.; Schulten, E.; Alia; Gast, P.; Raap, J.; Lugtenburg, J.; Hoff, A. J.; de Groot, H. J. M. *Biol. Chem.* **2001**, *382*, 1271−1276.
(58) Herzfeld, J.; Berger, A. E. *J. Chem. Phys.* **1980**, *73*, 6021−6030.
(59) Bonnerjea, J.; Evans, M. C. W. *FEBS Lett.* **1982**, *148*, 313−316.

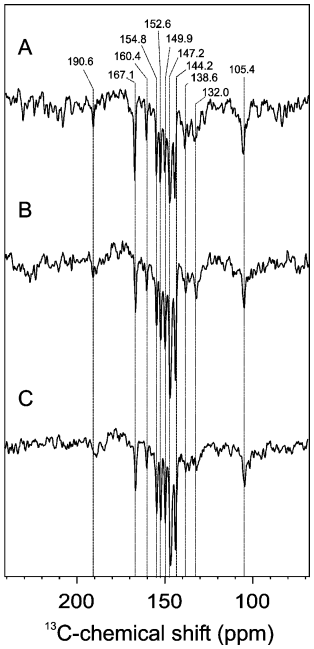

Figure 3. ^{13}C MAS NMR spectra of PS1−110 particles obtained at 223 K under continuous illumination with white light at MAS frequency of 6.4 kHz (A), 8.0 kHz (B) and 9.0 kHz (C). Assigned centerbands are visualized by the dashed lines.

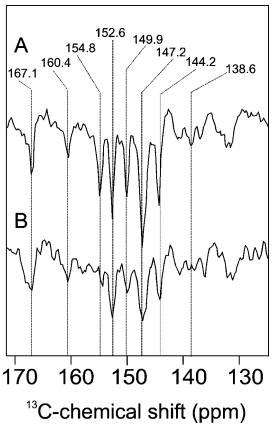

Figure 4. ^{13}C MAS NMR spectra of PS1 particles obtained at 223 K under continuous illumination with white light. PS1−110 (A) and PS1−CPI (B) particles at MAS frequency of 3.6 kHz. In both spectra, a line-broadening factor of 50 Hz has been applied. Assigned centerbands are visualized by the dashed lines.

does not produce electronic triplets, from such an electronic structure, no photo-CIDNP can be expected. Therefore, it is reasonable to assume that the observed photo-CIDNP enhancement originates from the radical pair P_{700}^{+} A_0^{-}. In contrast to PS2, having a Pheo *a* as primary electron acceptor, photo-CIDNP is produced in PS1 by a radical pair formed by two Chl *a* molecules.

The Sign. The difference between a Chl *a* radical anion in PS1 and a Pheo *a* radical anion in PS2 may also be responsible for change of the sign of the photo-CIDNP enhancement, the most obvious difference between both RCs. Recent EPR data on PS1 suggest that the isotropic *g* value of the Chl *a* acceptor anion radical[60,61] is closer to the isotropic *g* value of the P700 donor cation radical[62−64] than for the corresponding donor and acceptor in PS2 and in bacterial reaction centers. A smaller Δg causes a smaller contribution of the DD mechanism to the nuclear polarization and simultaneously a larger contribution of the TSM mechanism. Hence it is possible that the TSM contribution dominates for PS1, which would explain why all signals have the same sign. For the DD contribution, the sign depends on the sign of several parameters and may even depend on orientation, while for the TSM contribution the sign depends only on the sign of the coupling between the two electron spins.[39] According to the sign rules, an emissive TSM contribution implies that the coupling between the two electron spins is negative. Measurements of this coupling and of the *g* tensor of the Chl *a* radical anion by high-field EPR would be required to experimentally support or refute this hypothesis.

Table 2. Deviations between the *g* Tensors of a Chlorophyll a Anion Radical Chl A-· and a Pheophytin Anion Radical Pheo-· with Analogous Geometric Structure (DFT computations with ADF ZORA). the Directions of the Principal Axes Deviate by $\Delta\theta$.

	g_{11}	g_{22}	g_{33}	g_{iso}
Chl $a^{-\bullet}$	2.00461	2.00317	2.00206	2.00328
Pheo$^{-\bullet}$	2.00415	2.00308	2.00211	2.00311
$\Delta\theta$	4.2°	2.6°	3.3°	

Earlier work demonstrated that DFT computations of the *g* tensor of bacteriopheophytin acceptor anion radicals within the ZORA formalism were in good agreement with experimental values.[65] Such computations can also help to estimate differences between the *g* tensors of Chl *a* and Pheo *a* anion radicals. As is seen in Table 2, DFT predicts rather minor differences both in the principal values and in the principal axes directions. Thus, explanation of the sign change by changes in the *g* tensor of the acceptor radical anion appears to be unlikely. In addition, our DFT results suggest that the experimental isotropic *g* values for the Chl *a* anion radical[60,61] still have limited precision.

Alternatively, the change of the sign of the photo-CIDNP enhancement might be explained on the basis of the anisotropy of photo-CIDNP. In entire bacterial photosynthetic units containing selectively isotope labeled cofactors again a sign change occurred which has been tentatively explained by self-orientation of the membrane-bound proteins induced by sample spinning around the magic angle before freezing.[34] Due to the strong anisotropy of photo-CIDNP, oriented RCs are expected to show a enhancement pattern that is different from randomly oriented samples. For the sample containing the PS1−110 membrane complex, such a self-orientation effect cannot be ruled out. However, the observation of a similar enhancement pattern in the smaller PS1−CPI sample makes this explanation unlikely.

Photo-CIDNP sign rules[39] suggest that the difference between PS1 and PS2 could then be related either to a substantial difference in the electron−electron coupling, which would also shift the balance between the DD and TSM mechanisms, or to a difference in the hyperfine tensors of those nuclei for which

(60) MacMillan, F.; Hanley, J.; van der Weerd, L.; Knüpling, M.; Un, S.; Rutherford, A. W. *Biochemistry* **1997**, *36*, 9297−9303.
(61) Rigby, S. E. J.; Muhiuddin, I. P.; Santabarbara, S.; Evans, M. C. W.; Heathcote, P. *Chem. Phys.* **2003**, *294*, 319−328.
(62) Kamlowski, A.; Zech, S. G.; Fromme, P.; Bittl, R.; Lubitz, W.; Witt, H. T.; Stehlik, D. *J. Phys. Chem. B* **1998**, *102*, 8266−8277.
(63) Berthold, T.; Bechtold, M.; Heinen, U.; Link, G.; Poluektov, O.; Utschig, L.; Tang, J.; Thurnauer, M. C.; Kothe, G. *J. Phys. Chem. B* **1999**, *103*, 10733−10736.
(64) Bratt, P. J.; Poluektov, O. G.; Thurnauer, M. C.; Krzystek, J.; Brunel, L.-C.; Schrier, J.; Hsiao, Y.-W.; Zerner, M.; Angerhofer, A. *J. Phys. Chem. B* **2000**, *104*, 6973−6977.
(65) Dorlet, P.; Xiong, L.; Sayre, R. T.; Un, S. *J. Biol. Chem.* **2001**, *276*, 22313−22316.

nonequilibrium polarization is observed. Because of the broadly similar geometry of the reaction centers, the dipole−dipole coupling between the electron spins is only slightly different. No information is available on the exchange coupling in PS1, and reliable computations of this parameter are not yet possible. Our DFT computations suggest that the SOMOs of the acceptor radical anions are rather similar (data not shown), but given the lower symmetry of the donor in PS2, the SOMO of P700 is likely to be different from the one of P680. If the former SOMO would have a stronger overlap with the acceptor SOMO, this would result in a larger exchange coupling and thus in a larger TSM contribution. As discussed above, a larger TSM contribution would explain the uniform sign of the photo-CIDNP enhancements in PS1. As the spatial and electronic structure of the radical pair state of the whole reaction centers cannot be modeled precisely enough with current quantum-chemical approaches, these considerations remain somewhat speculative, however.

Finally, differences in the hyperfine couplings can give rise to photo-CIDNP sign and intensity changes. This point will be further elaborated after discussing the assignment of the NMR lines.

Line Width and Intensities. The narrow line width of ≈60 Hz provides evidence for a rather rigid, ordered as well as structurally and electrostatically stable donor site without structural heterogeneities. Previous MAS NMR studies revealed similar properties of the donor site in bacterial RCs.[66] It appears to be a general property of RCs to have a rigid donor side, keeping reorganization energies of electron-transfer low.

The photo-CIDNP intensities of PS1 appear to be higher than in unlabeled RCs of bacteria and PS2. In addition to the narrow line widths, the photo-CIDNP signals may appear to be stronger due to a modified proportion of the two mechanisms producing nuclear enhancement. The predominating influence of the TSM over the DD mechanism in the stronger photo-CIDNP of PS1, as proposed in the present paper, would imply that both mechanisms cause opposite effects under current conditions. In fact, this was also suggested by the model computations in ref 39.

The Chemical Shifts. The observed twelve photo-CIDNP signals appear between 200 and 90 ppm. In this region, an almost complete set of preliminary assignments can be obtained. In agreement with previously measured photo-CIDNP spectra of unlabeled RCs of bacteria and of PS2, no aliphatic carbons have been observed. The moderately high spinning frequency achieved here allows for the first time for unequivocal detection of a carbonyl response of the aromatic macrocycle in a photo-CIDNP MAS NMR spectrum. The absence of aliphatic carbons is due to their weak coupling to the electron pair. Similarly, the vinylic carbons C-3^1 and C-3^2 as well as the carbonyls C-13^3 and C-17^3 do not appear. There are no signals that can be attributed to amino acids of the surroundings.

The photo-CIDNP data provide a set of Chl-*a* resonances, which can be assigned to a single Chl-*a* cofactor. Since in PS-1 both the donor and the primary acceptor are Chl-*a* cofactors, we cannot completely exclude the possibility that the spectrum contains contributions from both the donor and acceptor cofactors on the basis of only the chemical shifts. However our calculations suggest the appearance of stronger ^{13}C photo-CIDNP NMR signals from the donor than the acceptor (see below). This spectral predominance has also been observed in selectively isotope labeled bacterial RC, in which an unambiguous assignment was possible.[33] Experiments with oriented or ^{15}N-isotope labeled PS1 samples may provide empirical evidence for this assignment.

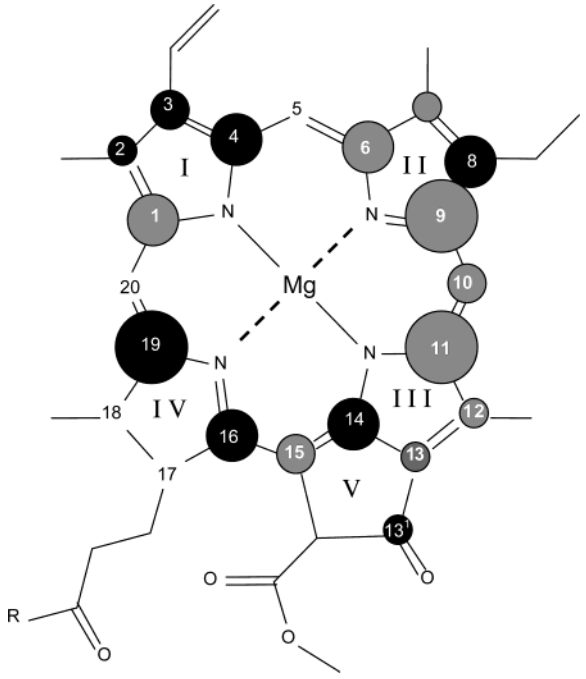

Figure 5. Photo-CIDNP patterns of Chl a molecules observed in PS1. The size of the circles is semiquantitatively related to the signal intensity. All observed photo-CIDNP enhanced NMR signals are negative (emissive). The black circles indicate unequivocal assignment, the gray circles rely on signals assigned to two or three carbons (Table 1).

The assignment of observed carbon resonances allows for a semiquantitative reconstruction of the electron-spin density pattern of π radical ions from the photo-CIDNP intensities of the observed Chl *a* (Figure 5), as these intensities scale with the anisotropy of the hyperfine coupling. Since both the strong signals at 154.8 (C-1 and C-6) and 147.2 ppm (C-9 and C-11) are assigned to two carbons each, some uncertainty remains in the pattern. The pattern appears slightly asymmetric mainly due to the absence of photo-CIDNP intensities on the methine carbons 5 and 20. Comparison of the photo-CIDNP patterns in PS1 and PS2[35] shows enhancement for mainly the same atoms. Carbons C-2, C-4, C-8, and C-13^1 appear in PS1 but have not yet been detected in PS2. Especially the high intensities of C-4 and C-8 in PS1 are significant differences to PS2.

Such an electron-spin density pattern correlates the electronic structure in the radical pair state of the reaction center to the chemical shift information that pertains to the ground state. As the electronic structures of the donor and acceptor Chl *a* are similar in the ground state but different in the radical pair state, the pattern provides additional information with respect to the assignment of the carbons to the donor or acceptor. To utilize this information, we compare computed ^{13}C hyperfine anisotropies of the Chl *a* cation radical as a simple model of the donor and of the Chl *a* anion radical as a model of the acceptor (Figure 6). Photo-CIDNP enhancement is strongly correlated to hyperfine anisotropy, but not simply proportional to it, as isotropic

(66) Fischer, M. R.; de Groot, H. J. M.; Raap, J.; Winkel, C.; Hoff, A. J.; Lugtenburg, J. *Biochemistry* **1992**, *31*, 11038−11049.

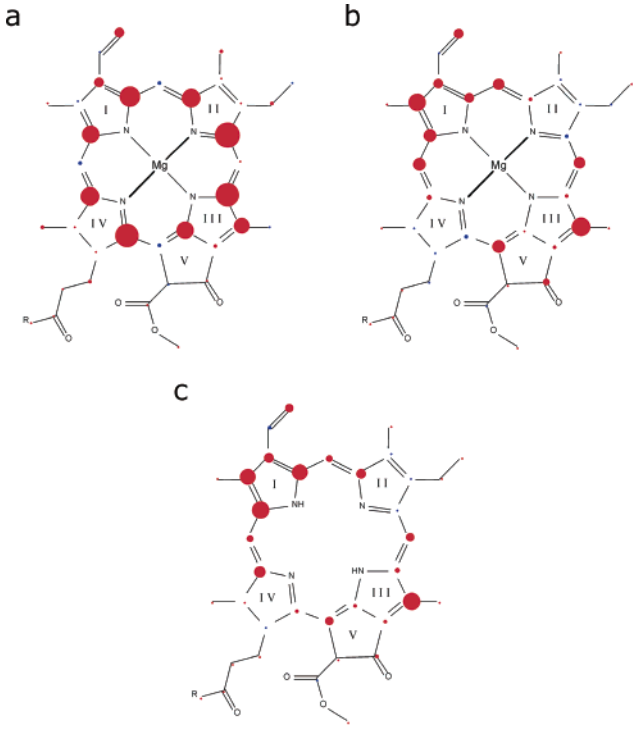

Figure 6. Hyperfine anisotropy of ^{13}C nuclei in radical species related to PS1 and PS2 (DFT computations). a) Chl *a* radical cation as a model for the donor. b) Chl *a* radical anion as a model for the acceptor in PS1. c) Pheo radical anion as a model for the acceptor in PS2.

hyperfine coupling and the relative orientation of both the *g* and the hyperfine tensor play a minor role.[39] Despite the latter complication, we may conclude from a comparison of Figures 5 and 6 that most of the signals very likely originate from the donor, with the possible exceptions of the methine carbons C-10 and C-15 and the signal of C-2. If these signals are assigned to the acceptor, the common sign would suggest that the TSM mechanism dominates, as the sign for the DD mechanism depends on the sign of the *g* value difference,[39] which is different for the two constituent radicals. The signal at C-8 would not be expected for either the donor or the acceptor, but note that a Chl *a* cation radical may be only a rather crude model for the donor. It also cannot be ruled out that the signal at 144.2 ppm originates from an aromatic amino acid.

Comparison to PS2. Within the limits of the preliminary assignments, no significant differences in the chemical shift patterns of P700 and P680 can be recognized. The largest difference is observed at the carbon C-14 of 1.9 ppm. This carbon is located on rings III and V, which suggests that the differences between both primary donors are located on this moiety of the Chl cofactor. Differences on that part of the Chl *a* are expected to be involved into the main changes of the electronic structure causing the shift of the redox potenial to 1.2 V.[33] Therefore, it would be very interesting to compare the chemical shifts of the 13^1-carbonyl carbons in PS1 and PS2, but this signal has not yet been reported in PS2. In PS1, the resonance of the carbonyl C-13^1 appears at about 189 ppm, which suggests that there is no hydrogen-bond or chemical modification on that carbonyl function in PS1 (Table 1). The signal appears to be relatively broad which may be due to some mobility. The absence of hydrogen bonding on the electron-spin carrying donor cofactor is in line with its previous assignment to P2.

As in PS2, only a single resonance has been observed from the methine carbons. In view of its position and relative broadness, it has been assigned to both methine carbons C-10 and C-15. In both plant RCs, no photo-CIDNP signal is detected on methine carbons C-5 and C-20. Compared to PS2, the single methine signal appears about 1 ppm downfield. This may be due to a relatively higher photo-CIDNP intensity at C-10 than on C-15 in PS1 as compared to PS2. This would provide additional evidence for a shift of electron spin density from the pyrrole ring II to the pyrrole rings III/V in PS2. In the photo-CIDNP MAS NMR spectrum of PS2, the signal at 104.6 ppm is clearly the signal with the highest absolute intensity in the spectrum. In PS1, the signal at 105.4 ppm is weaker than several signals of other aromatic carbons. This observation may be linked to a stronger localization of electron spin density in P680 over a certain moiety, whereas it is broader distributed over P700. Such an interpretation may also explain the differences between the photo-CIDNP pattern and the pattern of ^{13}C hyperfine anisotropies. The DFT computations also suggest that differences in the electronic structure of the acceptors in both systems are rather minor (see Table 2 and Figure 6b,c).

The Chemical Shift Anisotropy. In previous studies, the determination of the CSA values were hampered due to the overlap of the absorptive high-field sidebands with the emissive centerbands, and vice versa. Increasing the MAS frequency to moderately high spinning rate allows separation of absorptive sidebands from emissive centerbands without elimination of the sideband pattern. The CSA pattern is in line with values characteristic for aromatic carbons,[67,68] as well as to values obtained from samples containing solid Chls (data not shown). A reevaluation of the ^{13}C photo-CIDNP data of RCs of bacteria[30,31] and PS2[35] indicates similar CSA pattern in these RCs.

Conclusion

In the photo-CIDNP data of PS1, all ^{13}C NMR signals appear to be emissive. A coherent picture emerged in the discussion: (i) The TSM, causing emissive signals, dominates over the DD mechanism. Since both mechanisms cause opposite sign of photo-CIDNP, the predominance of the TSM can also be responsible for the remarkable strength of the photo-CIDNP in PS1, whereas in the RCs of bacteria and PS2, both mechanisms are of comparable intensity. (ii) The origin of the predominance of the TSM in PS1 seems not to be a decreased Δg value but the differences in the hf coupling. A stronger overlap of the SOMOs of donor and acceptor can be related to the lower asymmetry of electron spin density distribution on P700 compared to P680. (iii) The photo-CIDNP signals can be assigned to a single Chl *a* molecule, which is probably the P2 cofactor of the primary donor P700. The predominance of the donor over the acceptor in the ^{13}C photo-CIDNP NMR spectrum is in line with our calculations and analogue to a clear assignment obtained in the bacterial RC.

Acknowledgment. The authors thank Prof. Clemens Glaubitz (Frankfurt) for exciting discussions. The help of Dipl.-Biol. A.

(67) Veeman, W. S. *Prog. NMR Spectrosc.* **1984**, *16*, 193−235.
(68) Metz, G.; Siebert, F.; Engelhardt, M. *Biochemistry* **1992**, *31*, 455−462.

Diller, S. Prakash, M.Sc., and J.G. Hollander is gratefully acknowledged. This work has been financially supported by The Netherlands Organization for Scientific Research (NWO) through Jonge Chemici award (700.50.521), an Open competition grant (700.50.004), and a Vidi grant (700.53.423) as well as by the Volkswagen-Stiftung (I/78010) to J.M.

JA048051+